International Journal of Fracture **126:** 1–16, 2004.

On the fracture toughness anisotropy of mechanically poled ferroelectric ceramics

CHAD M. LANDIS
Department of Mechanical Engineering and Materials Science, MS 321, Rice University, P.O. Box 1892, Houston, TX 77251-1892 (Phone: (713) 348-3609; Fax: (713) 348-5423; E-mail: landis@rice.edu)

Received 16 September 2003; accepted in revised form 26 January 2004

Abstract. In this paper an incremental constitutive theory for the deformation due to switching in ferroelectrics is applied to predict the fracture toughness anisotropy in these materials after mechanical poling. Mechanical poling of an initially unpoled specimen differs from electrical poling in that only mechanical stresses are applied to the material. Therefore, no electrical polarization can develop. After mechanical poling, for example by a uniaxial applied stress, the fracture toughness of a ferroelectric ceramic for cracks running parallel or orthogonal to the poling direction will differ. Finite element computations of the steady crack growth process have been carried out to quantify these differences. Results are generated for a range of constitutive properties for three crack growth directions with respect to the initial mechanical poling direction. The results are discussed in relation to available experimental data and to the toughness anisotropy due to electrical poling.

Key words: Ferroelectrics, fracture toughness anisotropy, finite element methods.

1. Introduction

The fracture behavior of ferroelectric ceramics is of considerable interest due to the application of these materials in piezoelectric actuators. With regard to the fracture properties of ferroelectrics, a great deal of attention has been focused on the influence of domain switching on the R-curve behavior. It is commonly accepted that domain switching results in increased toughening in ferroelectrics in much the same way that the phase transformation does in partially stabilized zirconia materials. As such, a number of 'transformation toughening' type models for ferroelectric switching have appeared, Zhu and Yang (1997), Yang and Zhu (1998), Yang et al. (2001), Reece and Guiu (2002), that directly follow the original modeling efforts of McMeeking and Evans (1982) and Budiansky et al. (1983) for phase transformation toughening.

The constitutive model used for domain switching in these transformation toughening models assumes that switching occurs at a well defined combination of electric field and mechanical stress. The specific form of this switching criterion is usually that proposed by Hwang et al. (1995). Once the criterion for switching is achieved the material attains a finite, predetermined level of irreversible remanent strain and polarization. Furthermore, the reversal or reorientation of the switching direction is not accounted for in any of the transformation toughening models. In effect, once switching occurs, these models assume that the domain structure is frozen into the material. It will be shown in this work that such assumptions may lead to incorrect qualitative determinations of the toughness anisotropy in poled ferroelectric ceramics.

While electrical fields and polarization have a considerable effect on the toughness of ferroelectrics, in this work only unpoled material specimens loaded by mechanical stress will be modeled. Hence the term 'mechanically poled' refers to a ferroelectric material that has been cooled from above the Curie temperature and then irreversibly deformed by a mechanically applied stress. *At no time are electric fields applied to the sample*. In this situation, the constitutive law for the material must supply the history of stress given the history of strain or visa versa. In contrast to the very approximate constitutive laws applied in the transformation toughening type models, the toughness computations carried out in this work rely on a phenomenological, incremental constitutive law for domain switching that has been verified against micromechanical simulations, Landis (2003a). The phenomenological theory allows for constitutive features such as the Bauschinger effect, asymmetry in the maximum remanent strains in tension versus compression, reverse switching and the reorientation of the remanent strain state. With regard to the highly non-proportional stress histories near a growing crack tip, the features of reverse switching and remanent strain reorientation are especially important. This constitutive law is then applied within steady-state finite element computations to determine the toughness enhancement due to switching in electrically non-polar but mechanically poled ferroelectric ceramics.

2. The constitutive model

The nonlinear constitutive response of ferroelastic ceramics is a result of the mechanism of domain switching. The constitutive model presented here is phenomenological in nature, but has been verified against self-consistent micromechanical simulations based on the model of Huber et al. (1999). In most of its features the constitutive law is analogous to metal plasticity constitutive theories with kinematic hardening, except the form of the hardening law is specific to ferroelectrics and has been developed based on micromechanical simulations, Landis (2003a).

In order to maintain simplicity, isotropic elastic response and linear kinematics will be assumed such that the stress-strain relations can be written as

$$\varepsilon_{ij} = \frac{1+\nu}{E}\sigma_{ij} - \frac{\nu}{E}\sigma_{kk}\delta_{ij}\left(\varepsilon^r_{ij} - \varepsilon^0_{ij}\right) \tag{2.1}$$

Here, ε_{ij} are the Cartesian components of the infinitesimal strain tensor as referenced from the initial remanent strain state ε^0_{ij}, σ_{ij} are the Cartesian components of the Cauchy stress tensor, ν is the Poisson's ratio and E is the Young's modulus. Also, ε^r_{ij} are the Cartesian components of the total remanent strain tensor. The remanent strain is the irreversible strain and can also be referred to as the plastic strain. In all cases discussed in this paper, the datum for the total remanent strain ε^r_{ij} and the initial remanent strain ε^0_{ij} corresponds to the state of the material as cooled from above the Curie temperature, i.e. a thermally depoled sample. In this reference state, all possible domain orientations are equally likely. Prior to the fracture simulations the material will be pre-strained to ε^0_{ij} such that it is natural to choose this state as a new datum for the strain. However, within the implementation of the constitutive law the knowledge of this pre-strained state must always be retained and incorporated into the total remanent strain as referred to the as-cooled state.

The purpose of the nonlinear constitutive law is to provide the evolution of the remanent strain history given the stress or total strain history. Consistent with the facts that domain switching gives rise to only deviatoric strains and ferroelastic ceramics exhibit kinematic

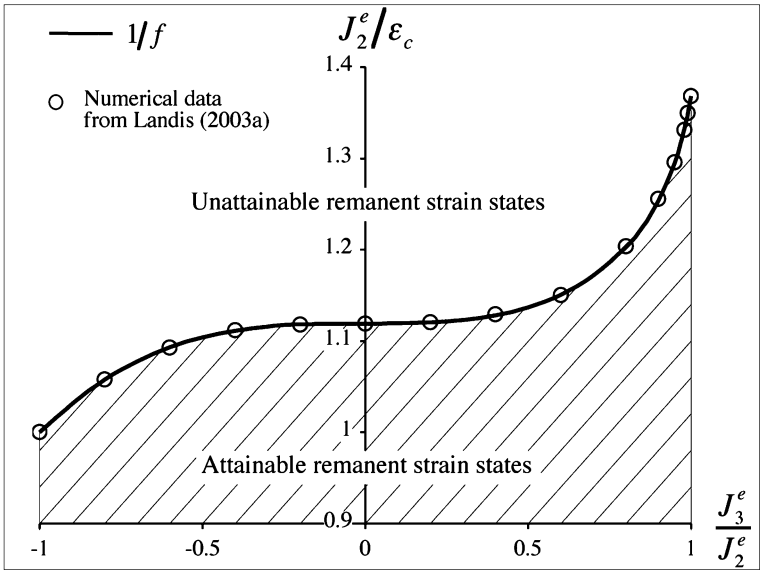

Figure 1. The region of attainable multi-axial remanent strain states (shaded area) for a polycrystal comprised of randomly oriented tetragonal single crystals. The solid curve represents the fitted equation given by Eqs. (2.7) and (2.8) and the circles are numerical simulation points from Landis (2003a).

hardening effects, it is assumed that the material responds elastically within a switching surface Φ described by

$$\Phi = \frac{3}{2}\left(s_{ij} - s_{ij}^B\right)\left(s_{ij} - s_{ij}^B\right) - \sigma_0^2 = 0. \tag{2.2}$$

If the stress state is on the switching surface and the load increment induces remanent straining, then the remanent strain increment is normal to the switching surface such that

$$\dot{\varepsilon}_{ij}^r = \lambda\left(s_{ij} - s_{ij}^B\right) \tag{2.3}$$

Here s_{ij} are the components of the stress deviator such that $s_{ij} = \sigma_{ij} - \delta_{ij}\sigma_{kk}/3$, s_{ij}^B are the components of the deviator of the back stress tensor σ_{ij}^B, σ_0 is the initial switching strength of the material in tension or compression, and λ is the as yet undetermined plastic multiplier.

The back stress tensor leads to kinematic hardening and must be used to enforce the remanent strain saturation conditions. The approach used to determine the back stresses is based on the assumption that the internal state of the ferroelastic material is completely characterized by the components of the remanent strain tensor, Cocks and McMeeking (1999) and Landis (2002). This assumption leads to the identification of a remanent potential, $\Psi^r(\varepsilon_{ij}^r)$, such that the back stresses are derived from the potential in the following manner

$$\sigma_{ij}^B = \frac{\partial \Psi^r}{\partial \varepsilon_{ij}^r} \tag{2.4}$$

In order to complete the constitutive theory, the form of Ψ^r must be specified. The primary role of the back stresses is to account for the strain saturation conditions in the ferroelastic material. As mentioned in the Introduction, ferroelectric ceramics exhibit an asymmetry in the attainable levels of remanent strain in tension versus compression, Fett et al. (1998). Figure 1

illustrates the remanent strain states that are possible in a ferroelastic polycrystal comprised of unpoled randomly oriented single crystal grains with tetragonal crystal structure. These results were obtained from micromechanical simulations and have been reported in Landis (2003a). Remanent strain states that are below the curve are possible in the material, while those above the curve are unattainable. Note that the following remanent strain invariants are used to describe the remanent strain space,

$$J_2^e = \left(\frac{2}{3} e_{ij}^r e_{ij}^r\right)^{1/2} \quad \text{and} \quad J_3^e = \left(\frac{4}{3} e_{ij}^r e_{ij}^r e_{ki}^r\right)^{1/3}. \tag{2.5}$$

Here, e_{ij}^r is the remanent strain deviator, $e_{ij}^r = \varepsilon_{ij}^r - \delta_{ij}\varepsilon_{kk}^r/3$. Only two invariants are required since the remanent strain is volume conserving. The magnitude of the remanent strain can be represented by J_2^e, and the type of remanent strain-state is designated by the ratio J_3^e/J_2^e. When J_3^e/J_2^e is -1 the remanent strain is an axisymmetric contraction, 1 corresponds to axisymmetric extension, 0 to pure shear remanent strain, and all other remanent strain states can be characterized within the range $-1 \leq J_3^e/J_2^e \leq 1$.

In order to describe the saturation states a strain-like variable $\overline{\varepsilon}$ is defined as

$$\overline{\varepsilon} = J_2^e f\left(J_3^e/J_2^e\right), \tag{2.6}$$

where

$$f\left(\frac{J_3^e}{J_2^e}\right) = -0.0965\left(\frac{J_3^e}{J_2^e}\right)^3 + 0.01\left(\frac{J_3^e}{J_2^e}\right)^6 + 0.8935, \quad \text{for} \quad \left(\frac{J_3^e}{J_2^e}\right) < 0 \tag{2.7}$$

and

$$f\left(\frac{J_3^e}{J_2^e}\right) = -0.1075\left(\frac{J_3^e}{J_2^e}\right)^3 - 0.0027\left(\frac{J_3^e}{J_2^e}\right)^6 - 0.028\left(\frac{J_3^e}{J_2^e}\right)^{21} + 0.8935, \quad \text{for} \quad \left(\frac{J_3^e}{J_2^e}\right) \geq 0 \tag{2.8}$$

Here, $1/f$ is a functional fit to the numerical results obtained from the micromechanical computations described in Landis (2003a). This fit is illustrated in Figure 1. When the remanent strain level characterized by $\overline{\varepsilon}$ reaches the compressive saturation level, ε_c, the remanent strain will be saturated. The only possible remanent strain states in the material are those that satisfy $\overline{\varepsilon} \leq \varepsilon_c$. Hence, in order to prohibit remanent strain states characterized by $\overline{\varepsilon} > \varepsilon_c$, the remanent potential Ψ^r must increase without bound as $\overline{\varepsilon} \to \varepsilon_c$. To enforce the strain saturation conditions the following remanent potential has been selected,

$$\Psi^r = \frac{1}{2} H_0 \varepsilon_c \left[\frac{J_2^e}{\varepsilon_c} \exp\left(\frac{m}{1 - \overline{\varepsilon}/\varepsilon_c}\right)\right]^2 \tag{2.9}$$

Here, H_0 is a characteristic level of back stress that primarily affects the initial slope of the uniaxial stress versus remanent strain curve, and m is another hardening parameter that controls how abruptly the strain saturation conditions are reached. Figure 2a illustrates the uniaxial stress versus remanent strain hysteresis curves for a few different sets of the material parameters H_0 and m. Figure 2b illustrates the uniaxial compressive stress-strain response of the model material with intermediate unloading paths. Note that within this theory, the Bauschinger effect does not set in until the applied uniaxial stress reaches a magnitude greater than $2\sigma_0$. In other words, unloading to zero stress for initial applied stress levels less than $2\sigma_0$

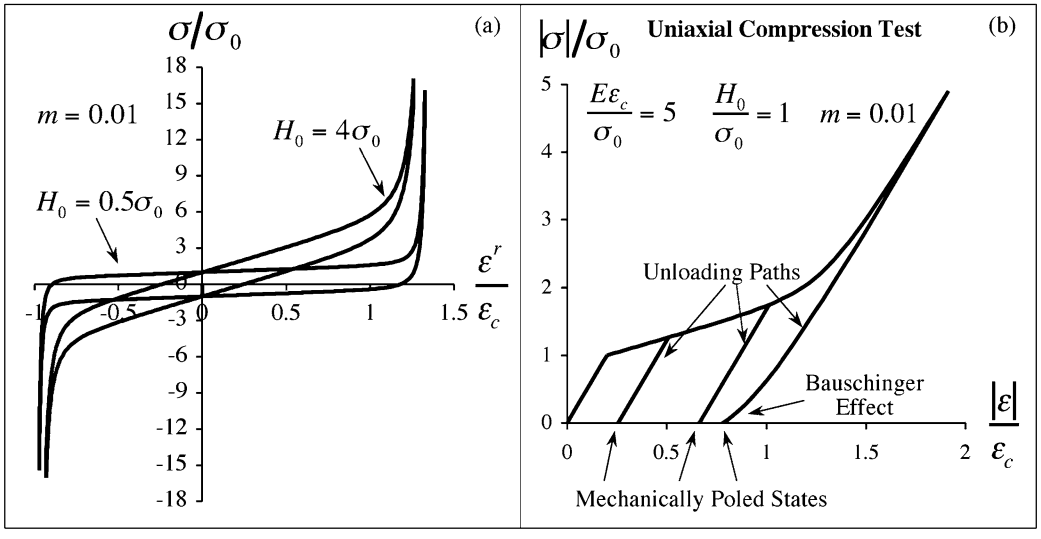

Figure 2. The mechanical stress-strain behavior of the model material. (a) The stress versus remanent strain hysteresis loops for two levels of the hardening parameter H_0. Notice the asymmetry in the levels of tensile and compressive strain that the material can attain. (b) The compressive stress versus compressive strain behavior with two intermediate unloading paths for the model material. Notice the Bauschinger effect that occurs when the initial applied stress is greater than $2\sigma_0$, and the three stress-free mechanically poled states.

is an entirely linear process. However, unloading to zero stress from above $2\sigma_0$ is accompanied by reverse switching, i.e. a Bauschinger effect.

With the remanent potential specified, it is possible to derive the back stresses and finally solve for the plastic multiplier yielding the incremental form of the constitutive law. For the implementation within the finite element model presented in the next section, a backward Euler integration scheme was developed such that the switching surface of Eq. (2.2) and the discretized version of the flow rule in Eq. (2.3) are satisfied at the end of the increment. Details of the backward Euler integration scheme can be found in Landis (2003b).

3. Mechanical poling and the fracture model

The fracture model implemented here is identical to that used in Landis (2003b) with the addition of an initial remanent strain due to mechanical poling. The constitutive law described in Section 2 will be applied within finite element computations to determine the ratio of the plateau level of the *R*-curve to the initiation toughness. These computations will be carried out for samples that are initially mechanically poled by a uniaxial applied stress. Figure 3 is a schematic of the sample configuration. The conceptual test procedure is as follows. An initially unpoled sample, i.e. as-cooled from above the Curie temperature, is mechanically poled by applying a uniaxial tensile or compressive stress to the material. The material need not be loaded entirely to the saturation level. For example, as illustrated in Figure 2b, the material can be loaded to a moderate stress level and then unloaded such that the resulting residual strain attains some intermediate magnitude. Next, a crack is introduced into the specimen in one of three orthogonal directions. These three directions are depicted on Figure 3. Once the crack is introduced, a Cartesian coordinate system is attached to the crack tip as shown in Figure 3, and the three initial poling directions will be termed ‘X-poled’, ‘Y-poled’ and ‘Z-poled’. The

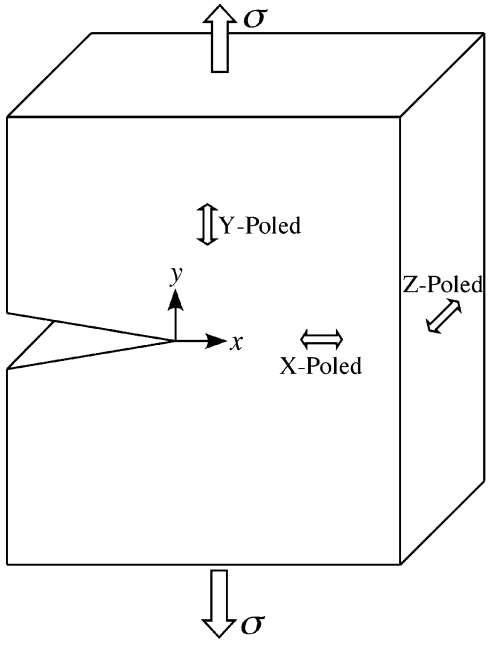

Figure 3. A schematic of the Mode I configuration to be modeled in this work. Any given sample will be poled in only one of the three depicted mechanical poling directions.

X-poled specimens will have initial remanent strain states of $\varepsilon^0_{xx} = \varepsilon_0$, $\varepsilon^0_{yy} = \varepsilon^0_{zz} = -\varepsilon_0/2$, $\varepsilon^0_{xz} = \varepsilon^0_{yz} = \varepsilon^0_{xy} = 0$, Y-poled specimens: $\varepsilon^0_{yy} = \varepsilon_0$, $\varepsilon^0_{xx} = \varepsilon^0_{zz} = -\varepsilon_0/2$, $\varepsilon^0_{xz} = \varepsilon^0_{xy} = 0$, and Z-poled specimens: $\varepsilon^0_{zz} = \varepsilon_0$, $\varepsilon^0_{xx} = \varepsilon^0_{yy} = -\varepsilon_0/2$, $\varepsilon^0_{xz} = \varepsilon^0_{xy} = 0$. In all cases mechanical poling consists of loading to cause remanent straining and then unloading to zero stress but non-zero residual strain.

Consider the following constitutive features of a mechanically poled specimen. Specifically, consider a specimen that is poled and unloaded along the second unloading path illustrated on Figure 2b. Under extreme levels of loading the amount of remanent strain achievable in compression for an *unpoled* sample is ε_c and that in tension is approximately $1.37\varepsilon_c$. For the second unloading path illustrated in Figure 2b the residual remanent strain is compressive and its magnitude is approximately $0.66\varepsilon_c$. Hence, after this initial poling, the amount of additional remanent strain the sample can attain in compression is $0.34\varepsilon_c$, but in tension the material can be irreversibly strained by $2.03\varepsilon_c$. It is important to remember this feature of the constitutive behavior when considering the fracture properties of the material. From a simplistic point of view, the crack will cause high tensile stresses in the y-direction ahead of the crack tip. If the material is able to accommodate these stresses by deforming in this direction then one should expect greater toughening increments than a material that can only respond to such stresses elastically. This explanation of toughening is overly simplistic because it does not consider the complex stress states around a crack or the fact that toughening occurs only after crack growth. However, this discussion has been included to give some sense of the response of a mechanically poled material.

Figure 3 illustrates a specific model geometry and loading, however this picture should only be taken as a schematic of a sample subjected to symmetric Mode I loading. In this work small scale switching will be assumed such that the representative height of the nonlinear

switching zone near the crack tip is much smaller than any other characteristic specimen dimension such as crack length, specimen width or ligament width. Furthermore, under plane strain conditions it is assumed that the specimen thickness is much greater than the switching zone size as well. The approximate half-height of the switching zone, R_s, is given as

$$R_s = \frac{1}{3\pi}\left(\frac{K_{\mathrm{I}}}{\sigma_0}\right)^2 = \frac{1}{3\pi}\frac{GE'}{\sigma_0^2} \tag{3.1}$$

Here K_{I} is the Mode I stress intensity factor such that within the small scale switching approximation, the stresses around the crack are given as

$$\left\{\begin{array}{c}\sigma_{xx}\\ \sigma_{yy}\\ \sigma_{xy}\end{array}\right\} \rightarrow \frac{K_{\mathrm{I}}}{\sqrt{2\pi r}}\cos\frac{\theta}{2}\left\{\begin{array}{c}1-\sin\frac{\theta}{2}\sin\frac{3\theta}{2}\\ 1+\sin\frac{\theta}{2}\sin\frac{3\theta}{2}\\ \sin\frac{\theta}{2}\cos\frac{3\theta}{2}\end{array}\right\} \quad \text{as} \quad r\rightarrow\infty \tag{3.2}$$

Here, r and θ represent a polar coordinate system centered on the crack tip, with θ measuring the angle between the radial direction and the x-axis. Under small scale switching conditions the prevailing mechanical conditions that govern the nonlinear behavior near the crack tip due to the geometry and far field loading of a sample are completely characterized by K_{I}. Furthermore, the applied energy release rate, G, is related to K_{I} as

$$G = \frac{K_{\mathrm{I}}^2}{E'}\,, \tag{3.3}$$

where $E' = E$ for plane stress and $E' = E/(1-\nu^2)$ for plane strain.

Within this model, crack propagation will be assumed to occur when the crack tip energy release rate G_{tip} reaches a critical value. In order to compute the relationship between the steady state far field applied energy release rate G_{ss} and G_{tip}, a steady state finite element formulation will be implemented (Dean and Hutchinson, 1980; Landis, 2003b). In the far field, tractions corresponding to Equation (3.2) are applied to the model and Equation (3.3) can be used to compute G_{ss}. Then, under steady-state conditions, G_{tip} can be calculated using Hutchinson's I-integral, Hutchinson (1974), as

$$G_{\mathrm{tip}} = I \equiv \int_{\Gamma}\left(Un_1 - \sigma_{ij}n_j u_{i,1}\right)\mathrm{d}s, \tag{3.4}$$

where Γ is a counterclockwise directed contour encircling the crack tip, n_i are the components of the unit normal directed to the right along the contour, u_i are the components of the displacement vector, and U is the history dependent stress work density at a material point defined by

$$U = \int_0^{\varepsilon_{ij}} \sigma_{ij}\mathrm{d}\varepsilon_{ij}. \tag{3.5}$$

Due to ferroelastic switching near the crack tip, the isotropic elastic solution for the stresses given by Equation (3.2) is only valid far from the crack. In order to compute the mechanical fields near the crack tip, and hence the ratio of G_{ss} to G_{tip}, a steady-state finite element procedure is implemented. This method was originally developed by Dean and Hutchinson

(1980) and applied to determine the mechanical fields near a growing crack in elastic-plastic materials. Recently it has been used by Landis (2003b) to determine the toughening due to ferroelastic switching in unpoled ferroelectrics. The formulation is based on the variational statement

$$\int_V \delta\varepsilon_{ij} C_{ijkl} \varepsilon_{kl} \mathrm{d}V = \int_S \delta u_i T_i \mathrm{d}S + \int_V \delta\varepsilon_{ij} C_{ijkl} \left(\varepsilon^r_{kl} - \varepsilon^0_{kl}\right) \mathrm{d}V, \tag{3.6}$$

where S is the boundary of the volume V, C_{ijkl} are the Cartesian components of the isotropic elastic stiffness tensor that can be written in terms of E and ν, and the tractions acting on the boundary S are given as $T_i = \sigma_{ji} n_j$. These tractions are determined from the stress field of Equation (3.2). After the application of the appropriate finite element interpolations and the cancellation of the appropriate variational term, the left-hand side of Equation (3.6) represents the linear elastic stiffness matrix dotted with the vector of unknown nodal displacements. Note that this stiffness matrix does not depend on any non-linear deformations, only on the finite element mesh geometry and elastic properties. The first term on the right-hand side represents the vector of known applied nodal forces. Finally, the second term on the right-hand side represents a body force vector due to the distribution of remanent strains in the material. Though not explicitly shown, Equation (3.6) must be solved by an iterative method. Initially, the remanent strain distribution is assumed to be $\varepsilon^r_{ij} = \varepsilon^0_{ij}$ at all points. The finite element equations due to Equation (3.6) are then solved and a new distribution of strains is obtained. The constitutive law described in Section 2 is then integrated along streamlines of constant height above the crack plane from $x = \infty$ to $x = -\infty$ using this new, but approximate, strain distribution to yield an updated approximation for the stress and remanent strain distributions. The new remanent strain distribution is then applied in Equation (3.6) and the solution procedure is repeated. This iterative procedure is continued until the solution for the nodal displacements, and hence the remainder of the mechanical fields, achieves a suitable level of convergence.

4. Results

The primary purpose of this study is to determine the anisotropy of the fracture toughness induced by mechanical poling of the material. In addition to these results, other features of the problem such as the distributions of stresses and strains around the crack tips and the sizes and shapes of the switching zones are of interest as well. In general, the normalized stress and remanent strain fields can be represented as

$$\frac{\sigma_{ij}}{\sigma_0} = \overline{\sigma}_{ij}\left(\frac{x}{R_s}, \frac{y}{R_s}; \frac{\varepsilon^0_{ij}}{\varepsilon_c}, \frac{\varepsilon_c E}{\sigma_0}, \frac{H_0}{\sigma_0}, m, \nu\right) \tag{4.1}$$

and

$$\frac{\varepsilon^r_{ij}}{\varepsilon_c} = \overline{\varepsilon}^r_{ij}\left(\frac{x}{R_s}, \frac{y}{R_s}; \frac{\varepsilon^0_{ij}}{\varepsilon_c}, \frac{\varepsilon_c E}{\sigma_0}, \frac{H_0}{\sigma_0}, m, \nu\right) \tag{4.2}$$

Here $\overline{\sigma}_{ij}$ and $\overline{\varepsilon}^r_{ij}$ represent dimensionless functions. These functions are fields as represented by their dependence on the x and y spatial coordinates, and they will also depend on the level of initial mechanical poling and the material properties as indicated by the dimensionless quantities appearing after the semicolon.

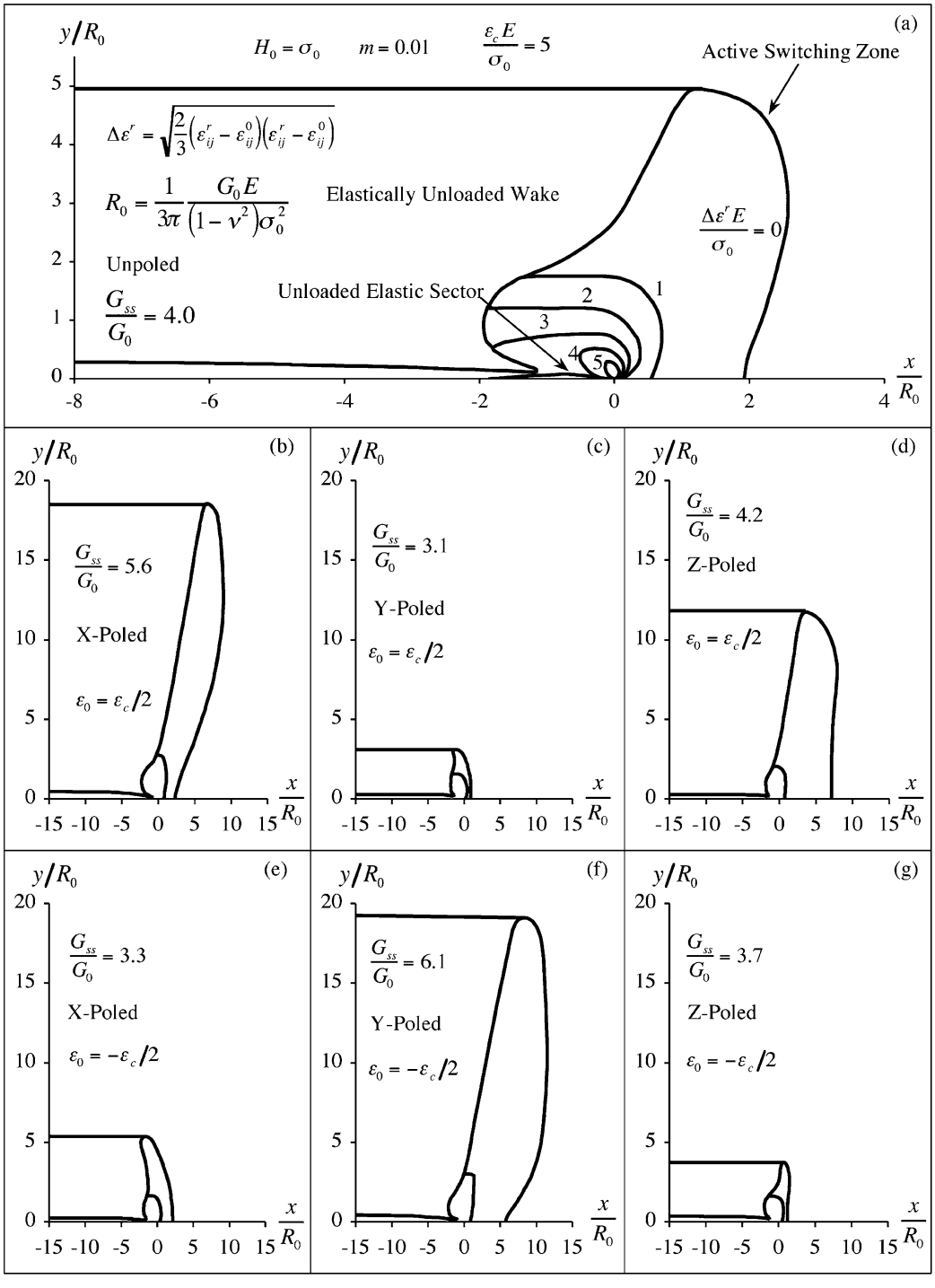

Figure 4. Switching zone sizes and shapes for both (a) unpoled and (b)–(g) mechanically poled cases. The material properties used to generate these results are $\varepsilon_c E/\sigma_0 = 5$, $H_0/\sigma_0 = 1$, $m = 0.01$ and $\nu = 0.25$. Detailed effective remanent strain contours are shown only on (a) the unpoled case. Graphs (b)–(g) show only two contours, one at the outer switching boundary and the second at the effective remanent strain level of $\Delta\varepsilon^r = \sigma_0/E$. Notice that the spatial coordinates are normalized by the characteristic switching zone size when the applied energy release rate reaches G_0, and the normalized steady state energy release rate is given on each plot.

Figure 4 illustrates the sizes and shapes of the switching zones around steadily growing cracks in (a) unpoled material, (b)–(d) material poled by a uniaxial tension, and (e)–(g) material poled by a uniaxial compression. In Figures 4b–g only two remanent strain contours are drawn corresponding to the outermost switching boundary and the location where the effective remanent strain is equivalent to σ_0/E. For the presentation of Figure 4, a new length scaling R_0 is introduced such that

$$R_0 = \frac{1}{3\pi}\frac{G_0 E'}{\sigma_0^2}. \tag{4.3}$$

If it is assumed that the critical crack tip energy release rate G_0 is a material property that does not depend on the initial mechanical poling state, then R_0 is constant for a given material, whereas R_s depends on the mechanical poling state. Note that at least to first order, transformation toughening type models predict that the switching zone size is directly proportional to the steady-state toughness G_{ss} and inversely proportional to σ_0^2 in a fashion similar to Equation (3.1). For the finite element results presented in this work, generally the size of the switching zone correlates with the macroscopic toughness G_{ss} of the material, in other words, the poling configurations depicted in Figures 4b, d and f are tougher than those shown in Figures 4c, e and g. However, the size of the switching zone is not directly proportional to G_{ss} as can be readily verified by comparing Figures 4d and 4g. Here the material of Figure 4d has a switching zone size greater than three times that of Figure 4g, but the ratio of the toughness for these materials is only 1.13. The reason for this loss of proportionality between the switching zone size and G_{ss} is that, due to hardening and the Bauschinger effect, the mechanical poling process can either increase or decrease the stress level where switching begins after the poling process. Take for example the compressive poling process depicted in Figure 2b. After initial loading and then unloading along the first path, the mechanically poled material will then switch in compression at a stress level of approximately 1.25 times σ_0. However, if this material were pulled in tension after the initial poling then the tensile switching stress would only be 0.75 times σ_0. Hence, the mechanical poling process can introduce an asymmetry in the initial switching strength of the material, which in turn, along with G_{ss}, affects the sizes and shapes of the switching zones near crack tips. Specifically, for the cases depicted in Figures 4d and 4g, from an investigation of the constitutive law, the effective in-plane switching stress for the case in Figure 4d is approximately $0.63\sigma_0$ and for the case in Figure 4g is $1.15\sigma_0$. Hence, if the applied G_{ss} were identical for these two cases then it is expected that the switching zone size for the case in Figure 4d should be approximately $1.15^2/0.63^2 \approx 3.3$ times larger than the zone size in Figure 4g. In fact, this is what is found from an inspection of Figures 4d and 4g. It is also important to note that mechanical poling also changes the levels of subsequent remanent strain the material can attain. However, this feature of the mechanical poling behavior primarily influences the switching zone size through its effect on G_{ss} which will be discussed in detail later in this section.

It is worth noting that the size of the switching zone contour where the effective remanent strain is equal to the characteristic elastic strain of σ_0/E is significantly smaller than the outer switching zone boundary. This illustrates the fact that large switching strains are confined to a region very close to the crack tip and the size of this region is only a fraction of R_s. Furthermore, note that the shapes of the switching zones depicted in these figures is that of the active switching zone. In other words, in the active switching zone, neighboring points at the same height above the crack plane have different remanent strains. Whereas, in the elastically unloaded wake or the unloaded elastic sector, neighboring points at the same height above

the crack plane have *identical* remanent strains. Lastly, material points outside of the active switching zone or the wake have remanent strain states equal to that of the initial mechanical poling state.

As mentioned previously, the primary result of each steady crack growth calculation is the ratio of the far field applied energy release rate, G_{ss}, to the crack tip energy release rate G_{tip}. Note that it is assumed that crack growth occurs when G_{tip} reaches the intrinsic fracture toughness of the material G_0. Hence the ratio G_{ss}/G_0 indicates the amount of toughening due to ferroelastic switching, with $G_{ss}/G_0 = 1$ corresponding to absolutely no toughening or R-curve behavior. In general G_{ss}/G_0 (which is equal to G_{ss}/G_{tip}) depends only on the dimensionless ratios of the material properties and the level of initial mechanical poling, i.e.

$$\frac{G_{ss}}{G_0} = \overline{G}\left(\frac{\varepsilon_{ij}^0}{\varepsilon_c}, \frac{\varepsilon_c E}{\sigma_0}, \frac{H_0}{\sigma_0}, m, \nu\right) \tag{4.4}$$

The prior work of Landis (2003b) investigated the effects of the last four dimensionless quantities on the toughening ratio for unpoled materials, $\varepsilon_{ij}^0/\varepsilon_c = 0$. The following qualitative dependencies were found. The toughening ratio G_{ss}/G_0 increases as the normalized saturation level of remanent strain $\varepsilon_c E/\sigma_0$ increases. This is to be expected since a greater propensity for remanent straining leads to more dissipation and higher toughening. The relative toughening decreases as the hardening of the material, either H_0/σ_0 or m increases. Again this is to be expected since a high hardening material tends to retard remanent straining and in turn decreases toughening. Lastly, there was found to be only a very weak dependence of G_{ss}/G_0 on Poisson's ratio ν. The work to be reported presently will investigate the relationship between G_{ss}/G_0 and the initial mechanical poling level for $\varepsilon_c E/\sigma_0 = 3$ and 5, $m = 0.01$, $\nu = 0.25$ and $H_0/\sigma_0 = 0.5$, 1 and 2.

Prior to presenting the results for the mechanically poled cases, it is informative to construct a reasonable hypothesis for the qualitative behavior of the relative toughening, taking the toughening in the unpoled case as a reference. Since crack tips tend to cause higher stresses in the y direction (for most polar angles around the tip) it is reasonable to assume that the materials propensity for remanent straining in the y direction will lead to greater toughening. For example, when a material is mechanically poled by a uniaxial compression in the y direction, domains switch from being aligned closely to the y direction to the x and z directions. Then, when a crack tip passes through with an accompanying large σ_{yy} component, the domains can switch back to the y direction causing dissipation and toughening. In contrast, a material poled by tension in the y direction will have most domains initially aligned closely with the y direction. Now when a crack tip passes nearby, these domains cannot switch again towards the y-axis and hence the dissipation due to domain switching will be decreased. Applying these considerations, one would expect the following qualitative rankings of toughening: Y-Poled in compression > Unpoled > Y-Poled in tension, X-Poled in tension > Unpoled > X-Poled in compression and Z-Poled in tension > Unpoled > Z-Poled in compression. Furthermore, at first glance, one would also expect that the toughening for comparable X and Z-Poled specimens would be similar since both of these orientations are perpendicular to the y direction.

Figures 5a–d plot the quantitative dependence of the toughening ratio G_{ss}/G_0 against the initial uniaxial remanent poling strain $\varepsilon_0/\varepsilon_c$ for each of the three poling directions, plane strain conditions, $\varepsilon_c E/\sigma_0 = 3$ and 5, $m = 0.01$, $\nu = 0.25$ and $H_0/\sigma_0 = 0.5$, 1 and 2. For all cases the unpoled state corresponds to $\varepsilon_0/\varepsilon_c = 0$. Note that the qualitative behavior of the Y-Poled and

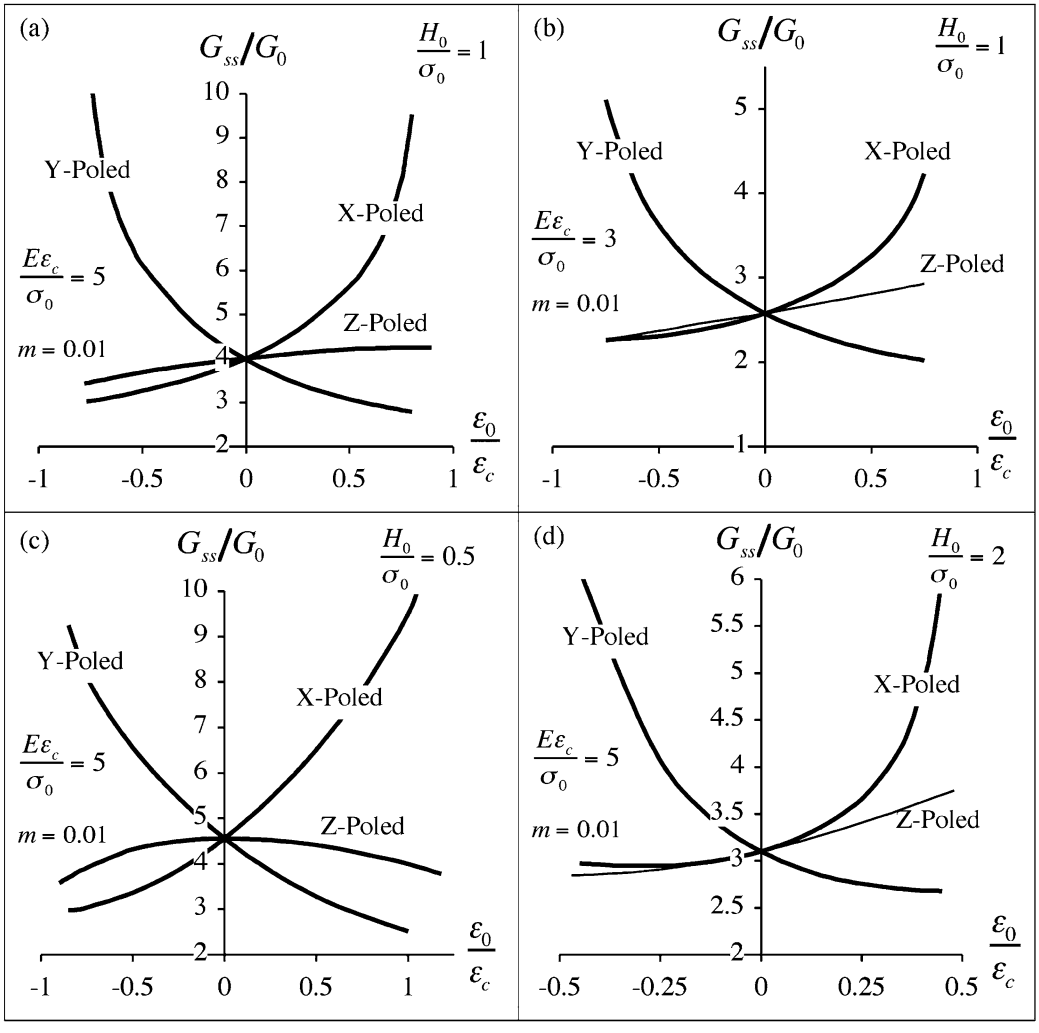

Figure 5. The normalized toughness enhancement G_{ss}/G_0 versus the initial mechanical poling strain for X, Y and Z-Poled samples for plane strain conditions and (a) $\varepsilon_c E/\sigma_0 = 5$ and $H_0/\sigma_0 = 1$, (b) $\varepsilon_c E/\sigma_0 = 3$ and $H_0/\sigma_0 = 1$ (c) $\varepsilon_c E/\sigma_0 = 5$ and $H_0/\sigma_0 = 0.5$ and (d) $\varepsilon_c E/\sigma_0 = 5$ and $H_0/\sigma_0 = 2$. For all cases $m = 0.01$ and $\nu = 0.25$.

X-Poled specimens is as hypothesized in the previous paragraph. However, the behavior of the Z-Poled material appears to be somewhat anomalous. In the soft material with $H_0/\sigma_0 = 0.5$, the Z-Poled materials in either compression or tension have toughness ratios less than that of the unpoled material. Higher hardening materials exhibit a qualitatively expected behavior with material poled in tension tougher than material poled in compression, but the quantitative effect of poling in the z direction is much smaller than might be expected from a comparison to the X-Poled material. Additional examples of the toughening due to Z-Poling are included in Figure 6a. Essentially the Z-Poled material has a toughening ratio similar to that of the unpoled material, whether it is poled in tension or compression.

The relatively weak dependence of the toughening ratio on the level of poling in the z direction can be explained by considering the out-of-plane constraint imposed by the plane strain conditions. Under plane strain conditions, the out-of-plane strain components equal

zero, i.e. $\varepsilon_{zz} = \varepsilon_{xz} = \varepsilon_{yz} = 0$. If domains switch completely from being oriented towards the z direction to an in-plane direction, as is assumed in transformation toughening type models, then this will cause a large negative remanent strain component ε^r_{zz}. In order to maintain a total out-of-plane strain of zero, the elastic strain must then be positive and have the same magnitude as ε^r_{zz}. This elastic strain component must arise from an out-of-plane stress component of a magnitude approximately equal to $E\varepsilon^r_{zz}$. Therefore, if $|\varepsilon^r_{zz}| > \sigma_0/E$ then the out-of-plane stress will be close to σ_0 and there will be a tendency for the domains to switch back towards the out-of-plane direction. The actual events do not proceed by switching in-plane and then switching back out-of-plane, but rather by switching only a relatively small amount. Hence, the out-of-plane constraint will negate the expected toughening effect described previously. Again, transformation toughening type models are not able to account for this kind of partial switching and its associated effects on fracture toughness. In order to verify that the out-of-plane boundary condition plays a significant role in the toughening of ferroelastic materials, computations were performed under *plane stress* conditions for a single set of material properties. The results of the plane stress simulations are presented in Figure 6b. These results indicate that under plane stress conditions, the material poled in the z direction exhibits a behavior as initially hypothesized. However, now the X-Poled material yields a very weak dependence of the toughening on the initial poling strain. Ultimately, the plane strain and plane stress results of Figures 5 and 6 illustrate the sensitivity of the *qualitative* toughening behavior of ferroelastic materials on the out-of-plane boundary conditions.

In summary, the results of this study have shown that in plane strain, significant toughness enhancements are achieved for materials that are initially mechanically poled by tension in the x direction or by compression in the y direction. In plane strain, mechanical poling in the out-of-plane direction induces only modest changes in the toughness enhancement with respect to the unpoled state. This somewhat counterintuitive result is explained by considering the out-of-plane constraint, and it was shown that under plane stress conditions significant toughness enhancements do occur for materials poled by tension in the out-of-plane direction. The sensitivity of the toughness anisotropy of ferroelastic materials to the out-of-plane boundary conditions leads to an important step in understanding the toughness of electrically poled ferroelectric materials and will be discussed in the next section.

5. Discussion

Ultimately, the viability of the model presented in this work can only be ascertained by a comparison with experimental observations. Unfortunately, to date there have been no experimental studies on purely mechanically poled ferroelectrics, and so a direct comparison of the model predictions to measurements is not possible. However, there have been studies on the fracture toughness anisotropy of *electrically* poled ferroelectrics, and with some careful considerations a limited comparison between this model and the experiments on electrically poled materials can be performed. The remainder of this discussion will focus on this comparison.

One of the motivating factors for this theoretical study is the experimental investigation of Lucato et al. (2000, 2002) on the fracture toughness anisotropy of electrically poled ferroelectrics. Lucato et al. (2002) measured the R-curve behavior of both unpoled and poled ferroelectric ceramics. The three electrical poling directions that were investigated in this study correspond to the mechanical poling directions illustrated in Figure 2. Due to the fact that fully coupled ferroelectric constitutive models are still in their infancy and remain un-

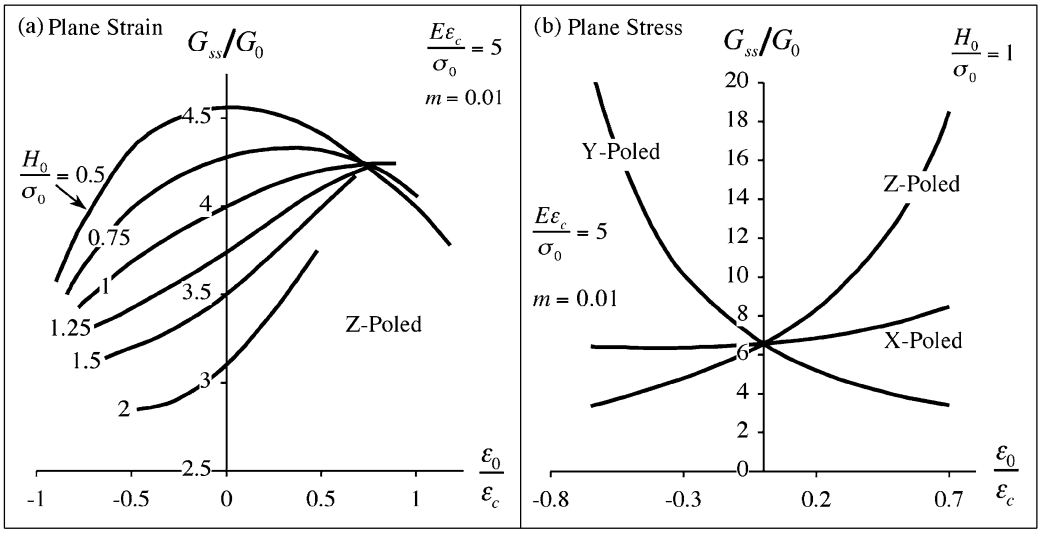

Figure 6. The normalized toughness enhancement G_{ss}/G_0 versus the initial mechanical poling strain for Z-Poled samples for (a) plane strain and a range of H_0/σ_0 from 0.5 to 2 and (b) plane stress conditions. Note that the effects of the out-of-plane boundary condition, i.e. plane stress versus plane strain, are considerable.

tested; the study in this work has focused on the simpler case of mechanically poled materials. A comparison of results generated for mechanically poled materials to observations on electrically poled samples must be performed with care and some physical insight. First, it is essential to realize that the electrical poling process creates a material that is piezoelectric, and furthermore the piezoelectric effect is aligned with the polarization direction. Hence, materials that are electrically poled in the x and y directions will not only have complex distributions of stress and strain near the crack tip, but also nontrivial distributions of electric field and electric displacement. Therefore, due to the in-plane piezoelectric effect, a comparison of mechanically poled computations in the X and Y-Poled configurations to observations on electrically poled materials is ill-advised and will not be carried out here.

In contrast to the in-plane poling cases, materials that are electrically poled in the z direction can exhibit in-plane isotropic elastic behavior under a restricted set of out-of-plane electrical boundary conditions. Therefore comparison of the out-of-plane mechanical poling case to the electrical poling case may be possible. Consider a material that is poled in the out-of-plane (i.e., z) direction. The piezoelectric and elastic properties of such a material are represented by third and fourth rank tensors that are transversely isotropic about the polarization direction. Therefore, for mechanical loading in the x-y plane the elastic response is isotropic in this plane. Furthermore, in-plane mechanical loads will lead to an electrical response due to the piezoelectric effect. The details of this electrical response depend on the electrical boundary conditions in the out-of-plane direction.

First, consider the case of a poled specimen with electrodes on the two faces perpendicular to the z direction. Furthermore we will consider the case where a wire connects the electrodes such that there is a short circuit boundary condition and the component of the electric field in the z direction must be equal to zero, $E_z = 0$. Now, applied mechanical loading in the x-y plane will cause changes in the electric displacement component D_z through both the piezoelectric effect and by ferroelectric switching. Near a crack the stresses and hence D_z will vary with both the x and y coordinate directions such that $D_z = D_z(x, y)$. Note that an

electric displacement field of the form $D_x = D_y = 0$ and $D_z = D_z(x, y)$ satisfies Gauss' law $D_{i,i} = 0$, and therefore no electrical fields will be generated in the x-y plane for the short circuit boundary conditions. Therefore, under short circuit conditions, in-plane mechanical loading leads to only out-of-plane electrical response through the electric displacement component D_z. No in-plane electrical fields will be generated for this set of out-of-plane boundary conditions. Hence, the in-plane mechanical behavior of an electrically Z-Poled sample may be approximated by the behavior of a mechanically Z-Poled sample.

Next, consider the case of a poled specimen with the electrodes removed from the faces perpendicular to the z direction. The electrical boundary conditions for this situation are far more complicated than those described previously. We will make the following assumptions when discussing this case. First, we assume that during the process of removing the electrodes from the z faces, free charges from the surroundings are able to attach to the surfaces such that the normal component of the electrical polarization is balanced, and no electric fields are required to enforce Gauss' law across the free surface. Second, during the application of in-plane mechanical loading these free charges that have attached themselves to the surface do not move. Finally, for the sake of simplicity, we will assume that the dielectric permittivity of the atmosphere surrounding the sample can be approximated as equal to zero. Given these assumptions, the electrical boundary condition in the z direction is that $D_z = P_0$, where P_0 is the remanent polarization induced by the initial electrical poling process. Now, during the application of in-plane mechanical stress, domain switching will cause changes in the remanent polarization in the z direction. However, in order to maintain D_z at a constant level of P_0, an electric field in the z direction must develop. In an analogy with the previous set of boundary conditions one might expect the spatial dependence of this electric field to have the form $E_x = E_y = 0$ and $E_z = E_z(x, y)$. However, an electric field distribution of this form does not satisfy $\nabla \times \mathbf{E} = 0$, i.e. electric field components of this form cannot be derived from a single scalar electric potential as required by Maxwell's laws. Therefore, for the case where the electrodes are removed from the sample, both out-of-plane *and* in-plane components of electric field and electric displacement will be generated by the application of applied in-plane stresses. Hence, this set of electrical boundary conditions does not admit only mechanical in-plane fields and a comparison of this situation to the mechanical poling case is ill-advised and will not be carried out here.

One final consideration must be applied when attempting to compare results for mechanical poling to those of electrical poling. The fact that electrical poling is accompanied by a tensile strain implies that the electrically poled cases can only be compared to samples poled mechanically in tension. From the results plotted in Figures 5a–c the computations described in this work predict that the toughness enhancement for Z-Poled specimens in tension can be modestly higher or lower than the toughening for unpoled samples depending on the hardening. For the cases where $H_0/\sigma_0 = 0.5$ to $H_0/\sigma_0 = 2$ the difference in steady state toughness between the unpoled and tension Z-Poled cases ranges from 17% to −20% respectively. The experimental observations of Lucato et al. (2002) indicate that the toughness enhancement for unpoled samples is approximately 15% greater than that for samples electrically poled in the z direction under short circuit electrical boundary conditions. Qualitatively, the model predictions and observations that Z-Poling provides only modest changes in toughness with respect to the unpoled case are in agreement.

Another qualitative agreement between the results generated in this work and the experimental observations of Lucato et al. (2002) is the significant effect of the through-thickness boundary condition. Comparison of Figure 5b to Figure 6b illustrates the very strong depend-

ence of the switch toughening effect on the out-of-plane mechanical boundary conditions. Analogously, Lucato et al. (2002) observed that the toughness of samples poled electrically through the thickness was significantly greater for samples under the no electrode configuration than those under short circuit conditions. As discussed previously the short circuit conditions give rise to planar variations of the fields, while the no electrode configuration allows for more complex three dimensional field variations. Ultimately these results suggest that a careful treatment of the out-of-plane boundary conditions must be incorporated in any model attempting to describe the switch toughening of ferroelectric ceramics.

Acknowledgement

The author would like to acknowledge support from the Office of Naval Research contract ONR N00014-03-1-0537.

References

Budiansky, B., Hutchinson, J.W. and Lambropoulos, J.C. (1983). Continuum theory of dilatant transformation toughening in ceramics. *International Journal of Solids and Structures* **19**, 337–355.

Cocks, A.C.F. and McMeeking, R.M. (1999). A phenomenological constitutive law for the behavior of ferroelectrics. *Ferroelectrics* **228**, 219–228.

Dean, R.H. and Hutchinson, J.W. (1980). Quasi-static steady crack growth in small scale yielding. In Fracture Mechanics, ASTM-STP 700, 383–405.

Fett, T., Muller, S., Munz, G. and Thun, G. (1998). Nonsymmetry in the deformation behavior of PZT. *Journal of Materials Science Letters* **17**, 261–265.

Huber, J.E., Fleck, N.A., Landis, C.M. and McMeeking, R.M. (1999). A constitutive model for ferroelectric polycrystals. *Journal of the Mechanics and Physics of Solids* **47**, 1663–1697.

Hutchinson, J.W. (1974). *On steady quasi-static crack growth*. Harvard University Report, Division of Applied Sciences, DEAP S-8.

Hwang, S.C., Lynch, C.S. and McMeeking, R.M. (1995). Ferroelectric/ferroelastic interactions and a polarization switching model. *Acta Materialia* **43**, 2073–2084.

Landis, C.M. (2002). Fully coupled, multi-axial, symmetric constitutive laws for polycrystalline ferroelectric ceramics. *Journal of the Mechanics and Physics of Solids* **50**, 127–152.

Landis, C.M. (2003a). On the strain saturation conditions in polycrystalline ferroelastic ceramics. *Journal of Applied Mechanics* **70**, 470–478.

Landis, C.M. (2003b). On the fracture toughness of ferroelastic materials. *Journal of the Mechanics and Physics of Solids* **51**, 1347–1369.

Lucato, S.L., Lupascu, D.C. and Rödel, J. (2000). Effect of poling direction on R-curve behavior in lead zirconate titanate. *Journal of the American Ceramic Society* **83**, 424–426.

Lucato, S.L., Lindner, J., Lupascu, D.C. and Rödel, J. (2002). Influence of electrical and geometric boundary condition on crack growth in PZT. *Key Engineering Materials* **206–213**, 609–612.

McMeeking, R.M. and Evans, A.G. (1982). Mechanics of transformation toughening in brittle materials. *Journal of the American Ceramic Society* **65**, 242–246.

Reece, M.J. and Guiu, F. (2002). Toughening produced by crack-tip-stress-induced domain reorientation in ferroelectric and/or ferroelastic materials. *Philosophical Magazine* **A82**, 29–38.

Yang, W. and Zhu, T. (1998). Switch toughening of ferroelectrics subjected to electric fields. *Journal of the Mechanics and Physics of Solids* **46**, 291–311.

Yang, W., Fang, F. and Tao, M. (2001). Critical role of domain switching on the fracture toughness of ferroelectrics. *International Journal of solids and Structures* **38**, 2203–2211.

Zhu, T. and Yang, W. (1997). Toughness variation of ferroelectrics by polarization switch under non-uniform electric field. *Acta Materialia* **45**, 4659–4702.